Thermec '97 Int. Conf. on Thermomechanical Processing of Steel and Other Materials, Wollongong, Australia, July 7-11, 1997. pp. 2279-2285.

SIMULATION OF THERMAL MECHANICAL BEHAVIOR DURING INITIAL SOLIDIFICATION

B. G. Thomas and J. T. Parkman

Department of Mechanical and Industrial Engineering
University of Illinois at Urbana-Champaign
1206 West Green Street
Urbana, IL 61801

Abstract

Mathematical models have been developed to predict temperature, stress, and shape development during initial solidification. The heat transfer model was run for typical casting conditions in the mold for typical thin slab and conventional continuous slab casters. The calculated temperatures were input to an elastic-viscoplastic finite-element stress model of the solidifying steel shell. This model features an efficient algorithm to integrate the highly non-linear constitutive behavior of steel at high temperature. The stress model includes the temperature and composition-dependent effects of phase transformation on both the thermal linear expansion / contraction behavior, creep behavior, and pseudo-strain due to flow in the liquid. Stress and strain distributions are calculated along a line through the shell thickness, assuming no shell bending or sticking to the mold. Results are compared for 0.044%C and 0.1%C steels and for both cooling conditions. The results provide insight into the formation of longitudinal surface cracks in continuous-cast steel.

Introduction

Most of the surface defects in continuous cast steel initiate during the early stages of solidification in the mold. These include surface depressions, longitudinal and transverse surface cracks. Although a body of empirical knowledge and theory exists to understand how they form, the exact mechanisms for many of these problems are still unclear.

Several studies have been made to investigate how cracks form during continuous casting of steel. It is well-known that the middle carbon or "peritectic" steels containing 0.1 - 0.2% C are more prone to depressions and longitudinal surface cracks during casting than other grades. [1-3] This was initially attributed to an inherent lower ductility of these grades. However, H. Suzuki et al. [4] performed isothermal tensile tests on in-situ melted and resolidified samples which showed that ductility decreases slowly but steadily with increasing carbon and residual alloy content. There was no special embrittlement problem with middle carbon steels. Embrittlement was attributed to the drop in solidus temperature caused by microsegregation of the alloying elements. This is consistent with the findings of Ye et al. [5] that middle carbon steel shells have a 2% macroscopic strain to failure, which is greater than other steels. Thus, the increased surface cracking tendency of middle carbon steels is now attributed to the peritectic reaction, and the phase transformation contraction from delta-ferrite to austenite. Clearly, an accurate calculation of stress and strain during initial solidification that included the effect of temperature and composition on the steel properties would be useful.

Model description

A transient, thermal-elastic-viscoplastic finite-element model, CON2D [6, 7] has been developed to follow the thermal and mechanical behavior of a section of the solidifying steel shell, as it moves down the mold at the casting speed. It is applied in this work to simulate stress and strain development in a typical 1-D slice, pictured in Figure 1.

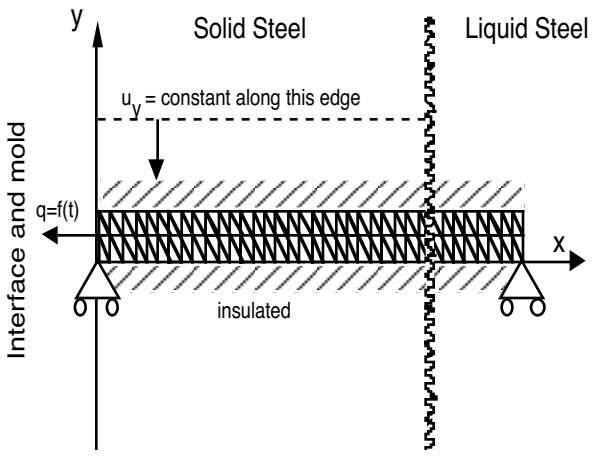

Fig. 1 - Model Domain and boundary conditions

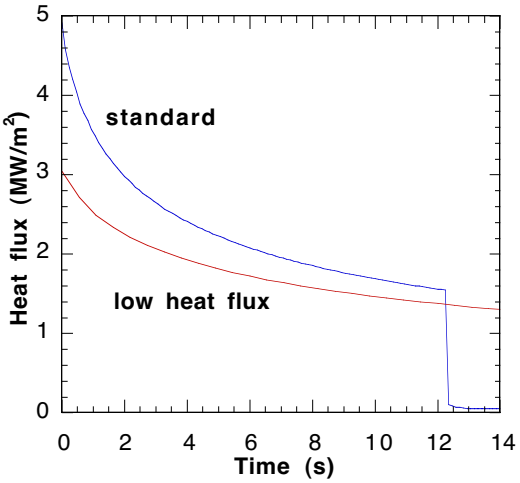

Fig. 2- Surface heat flux input to model

Heat Flow Model: The heat flow model solves the 2-D transient energy equation, using a fixed Lagrangian grid of 3-node triangles. Interfacial heat flux is input from another model, CON1D [8] which features a detailed treatment of the interfacial gap between the solidifying steel shell and the water-cooled copper mold. It includes mass and momentum balances on the solid and liquid powder layers. It also predicts the thicknesses and temperature distribution of the solidified and liquid powder layers, mold temperatures, and the heat flux distribution down the mold. The effects of oscillation mark size on both the powder consumption and heat transfer are also

incorporated. In this work, it was used to produce the heat flux curves in Figure 2, which correspond to typical conventional (low heat flux) and thin slab casting practices (high heat flux).

Stress Model: Starting with stress-free liquid at the meniscus, the stress model calculates the evolution of stresses, strains, and displacements, by interpolating the thermal loads onto a fixed-grid mesh of 6-node triangles. [6] The elastic strain rate vector, $\{\dot{\varepsilon}_e\}$, is related to the total strain rate vector, $\{\dot{\varepsilon}\}$, via:

$$\{\dot{\varepsilon}_e\} = \{\dot{\varepsilon}\} - \{\dot{\varepsilon}_T\} - \{\dot{\varepsilon}_{in}\} - \{\dot{\varepsilon}_f\} \qquad (1)$$

where $\{\dot{\varepsilon}_T\}$ is the thermal strain rate, $\{\dot{\varepsilon}_{in}\}$ is the inelastic strain rate in the solid, and $\{\dot{\varepsilon}_f\}$ is the pseudo-strain rate accounting for flow of the liquid. Friction between the mold and shell is neglected. Assuming that mold taper is not excessive, the surface shear stress generated by friction between the shell and the mold arises solely from ferrostatic pressure. Assuming there is no sticking of the shell to the mold, the maximum coefficient of friction is 1. Then, maximum friction stress in a 1-m long mold is: $\mu \rho g h = (1)\ (7000\ kg/m^3)\ (9.81\ m/s^2)\ (1m) = 68700$ Pa = 0.07 MPa. This stress is negligible relative to the thermal stresses, at least for times above 0.5 s. Thus, ignoring friction is reasonable unless these assumptions are not met.

The out-of-plane z-stress and the y-stress are both characterized by the state of generalized plane strain. This allows the 1-D simulations to reasonably estimate the complete 3-D stress state, for a long, wide, thin shell. This is the best assumption in the absence of bending or friction. Each slice is constrained by the rest of the shell to remain straight as it moves down the mold.

Elastic Strain: Stress is caused solely by elastic strain. The elastic modulus decreases with increasing temperature, based on data measured by Mizukami et al [9].

Thermal Strain: Thermal strains arise from volume changes caused by both temperature differences and phase changes (including both solidification and solid state transformations). They are calculated from the temperatures determined in the heat transfer analysis, {T}, and the state function TLE, or **t**hermal **l**inear **e**xpansion of the material. All strains, including those from phase transformations are assumed to be isotropic. For example, $\{\varepsilon_T\} = (\ TLE(T) - TLE(T_o)\ )\ \{1,1,0,1\}^T$. This neglects anisotropic effects, which may arise during columnar dendrite solidification. TLE is found from the temperature-dependent mass density. In mixed phase regions, TLE is found from a weighted average using the TLE curves for each of the individual phases present, based on their volume fractions. During steel solidification, liquid (l), delta ferrite (δ), austenite (γ), alpha ferrite (α) and iron carbide (Fe_3C) may be present:

$$TLE = (\%L)\ TLE_L + (\%\delta)\ TLE_\delta + (\%\gamma)\ TLE_\gamma + (\%\alpha)\ TLE_\alpha + (\%Fe_3C)\ TLE_{Fe3C} \qquad (2)$$

The TLE functions and phase fractions are calculated as a function of temperature and carbon content. The model adopts TLE functions for plain carbon steel, (Figure 3) based on solid phase density data by Harste [10] and liquid density data from Jimbo and Cramb. [11] Phase fractions are estimated using the equilibrium Fe-C phase diagram, so nonequilibrium undercooling due to slow nucleation kinetics is neglected.

Inelastic strain: Inelastic strain includes strain in the solid arising from both creep and plastic yielding. At high temperatures, important to stress development during solidification, the inelastic strain is dominated by creep, which is very sensitive to strain rate. Creep is significant even during a tensile test and cannot be distinguished from plastic strain. Thus, constitutive behavior for solidifying plain-carbon steel was simulated using the rate-dependent, elastic-viscoplastic model III of Kozlowski. [12] This model was developed to match tensile test measurements of Wray [13] and creep data of Suzuki [14] over a range of strain rates, temperatures, and carbon

contents to simulate austenite under continuous casting conditions. These equations were extended to model the enhanced creep rate in delta ferrite, and compare reasonably with tensile-test data from Wray, as shown in Figure 4.

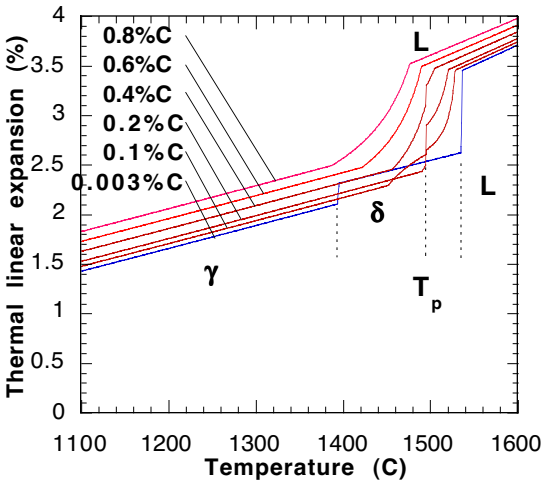

Fig. 3 - Thermal linear expansion of steel for different %C (data from Harste, Jimbo)

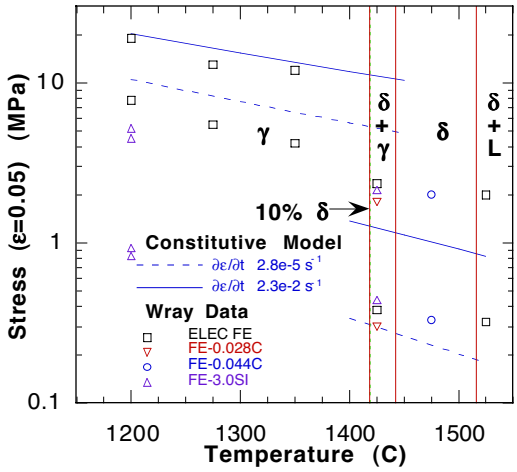

Fig. 4 - Comparison of predicted and measured (Wray) stress, showing δ-ferrite is weaker than γ

Flow Strain: The model assumes that when liquid is present, fluid flow will occur to exactly match the shrinkage. Elements are treated as liquid when any node in the element is above the specified coherency temperature (set to solidus). Liquid elements are set to have no elastic strain, and consequently develop no stress. The difference between the total strain and thermal strain in liquid elements is assumed to be made up by a "flow strain". This method allows easy tracking of various fracture criteria. For example, a large flow strain when the solid fraction is high indicates high cracking potential. It is also needed for future macrosegregation calculations.

Solution Details: This model features an efficient algorithm to integrate the highly non-linear constitutive equations. A new two-level solution algorithm has been implemented, which alternates between solutions at the local node point and the global system equations. [6] To minimize numerical errors, a very fine, graded mesh was required, including 201 nodes per row across the 20 mm wide shell. The time step size varies from 0.001s initially to 0.005s at 1s. Each 15s simulation needed about 10 minutes on an IBM RS6000-370.

Model Validation: The model has been validated with measurements from operating slab casters, and analytical solutions, described elsewhere. [6, 7]

Results

Effect of Carbon Content: Typical strain distributions are shown in Figure 5 for 0.1%C steel. At the surface, the inelastic and elastic strains are relatively small, so the total strain matches the thermal strain accumulated in the solid. Ideal taper calculations are therefore calculated reasonably based solely on the temperature of the surface. At the solidification front, liquid contraction exceeds solid shell shrinkage, causing flow into the mushy zone. It may be significant that 0.1% inelastic strain is accumulated in the solid during the δ to γ transformation. This occurs within the critical temperature range 20-60 ˚C below the solidus, where segregation can embrittle the grain boundaries, liquid feeding is difficult, and strain can concentrate in the thin liquid films. Figure 6 shows that lower carbon (0.044% C) steel also accumulates inelastic tensile strain during the δ to γ transformation shrinkage. However, this transformation begins 65 ˚C below the solidus in this steel, and there is virtually no inelastic strain generated in the weak delta phase. This effect may partly explain the better ductility of lower carbon steels. For both

steels, flow strain is generated primarily in the mushy zone, where the liquid is shrinking. Feeding is easy here, so this may not be significant. The low strains and generally similar behavior of these two grades, suggests that other phenomena may be important to cracks.

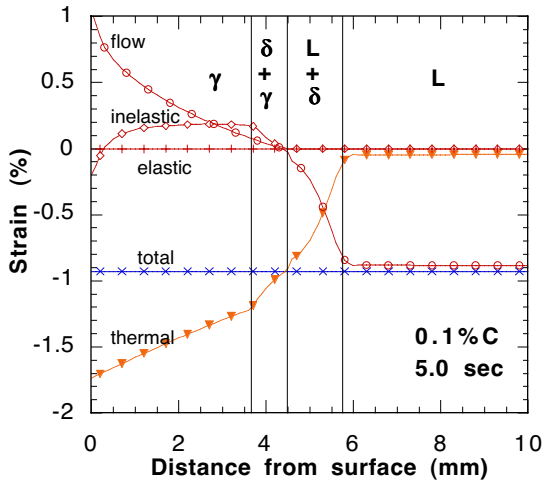

Fig. 5 - Typical strain distributions through shell thickness (0.1%C steel at 5 s below meniscus)

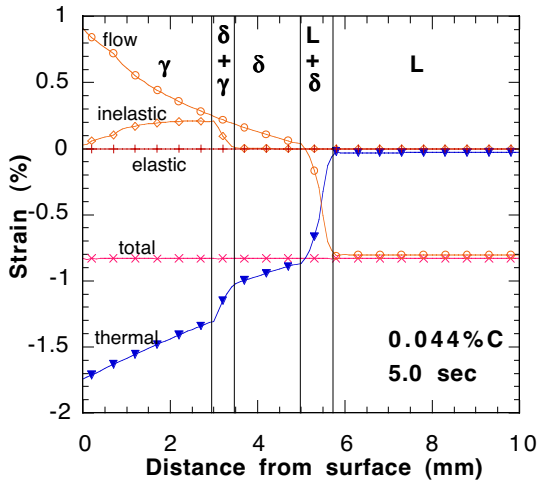

Fig. 6 - Strain distributions for 0.044%C steel

Effect of Cooling Rate: To alleviate longitudinal cracking, it has been proposed that heat flux from the shell to the mold be reduced at the meniscus. [15] This has led to higher viscosity mold powders for middle carbon steels. [16] Stress and inelastic strain profiles for high and low heat flux conditions are compared in Figure 7. In both cases, which have monotomic cooling, compression arises very quickly at the surface. This agrees with theory. [17] Note that average stress across the shell is always zero, which is required for equilibrium in the absence of sticking. About 40% of the way from the surface to the weak δ phase, the stress becomes tensile. Every frame of Figure 7 shows that both stress and inelastic strain are generated primarily during the δ to γ phase transformation. Liquid naturally solidifies stress free.

At 13s, the surface reheats below the mold by about 100 ˚C for the standard (high heat flux) case. This increases the compressive stress near the surface, with a corresponding increase in tensile stress in the austenite. The absolute strain and stress levels are not completely different between the two cases, even though it is believed that reheating greatly increases the likelihood of crack formation. [18] Yamanaka et al. [19] suggest that a crack will from when the total strain accumulated while the steel is between a solid fraction range from 0.8 to 0.99 exceeds 1.6%. Based on this data, surface cracks should not form in the mold in either case.

Longitudinal surface cracks might initiate within 1 second of the meniscus when the shell sticks to the mold (via problems with flux feeding, or mold taper problems). Here, non-uniform

Figure 7 - Comparison of stress and inelastic strain evolution for standard and low heat flux conditions in 0.1%C steel

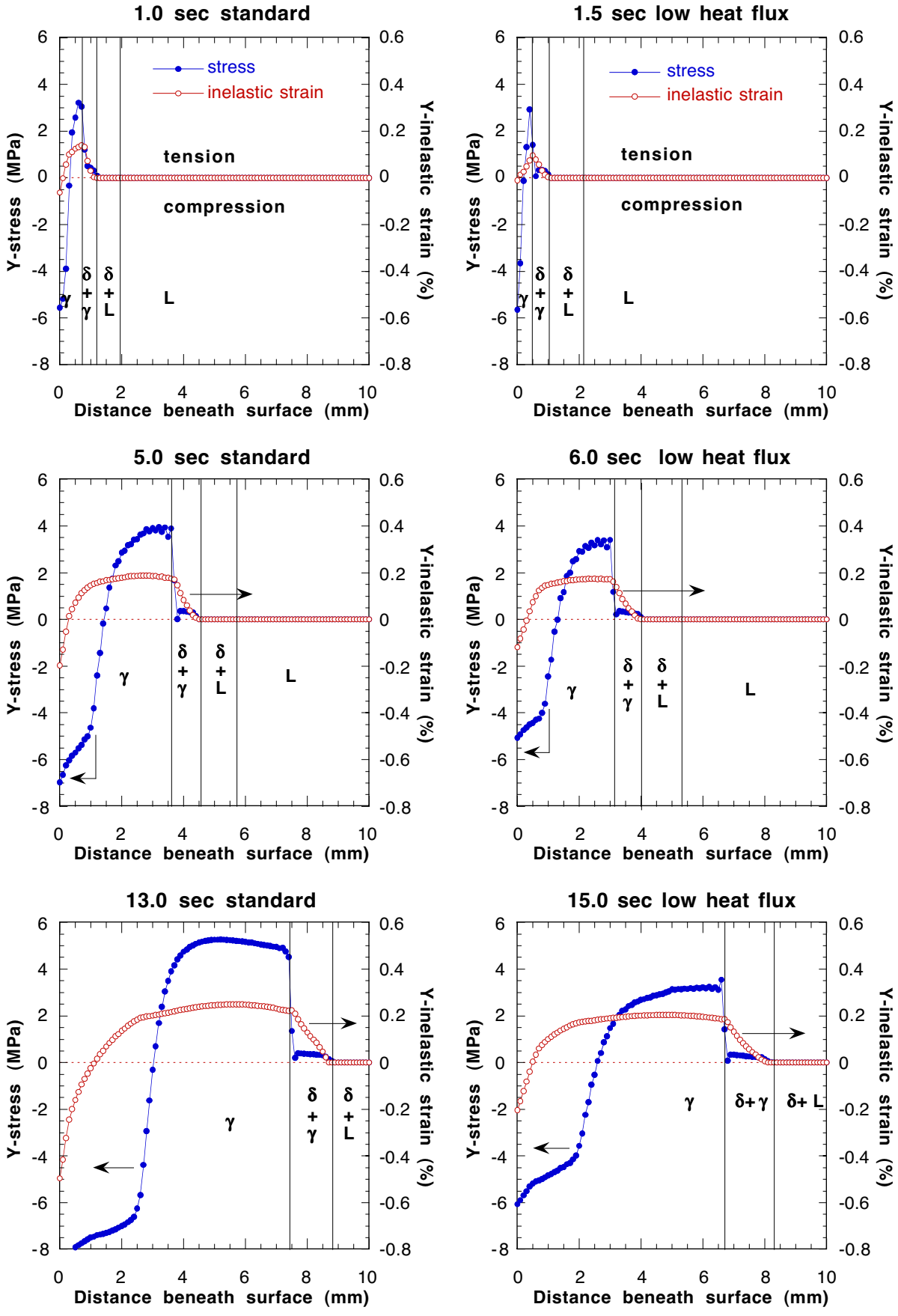

Fig. 7 - Comparison of stress and strain evolution in standard and low heat flux for 0.1%C steel

surface roughness will create local variations in heat transfer and shell growth rate. Strain concentrates in the hotter, thinner shell at the low heat flux regions. Localization may occur on both the small scale (at the segregated grain boundaries) and on a larger scale (within surface depressions or hot spots). Later sources of tensile stress (including constraint due to sticking, unsteady cooling below the mold, bulging, and withdrawal) worsen strain concentration and promote crack growth. Further work is needed to investigate these phenomena.

Conclusions

Transient finite-element model simulations have predicted the development of stress and strain in a solidifying steel shell. The findings suggest that:

1) Without sticking and with steady cooling conditions, the shell surface goes into compression within 1 s after solidification. Surface cracks grow only if these conditions are not met.
2) The δ-ferrite portion of the shell creeps very rapidly, which relaxes all of its stress. Thus, strain in this weak portion of the shell is controlled by the strength of the austenite portion.
3) Creep strain in the weak δ-ferrite and mushy portions of the shell is relatively small, because it is only needed to replace the elastic strain lost by stress relaxation.
4) In the absence of friction, the solid shell contracts on the order of 1% during the first 5s of solidification. The mismatch in shrinkage generates inelastic strains at the solidification front on the order of 0.1%, which should not be enough to cause to cracks. Thus, stress concentration and strain localization are required for cracks to form.
5) The sensitivity of cracks to carbon content and initial cooling rate appears more related to the formation of the non-uniform shell than to direct changes in stress and strain evolution.

Acknowledgments

The authors wish to thank the Continuous Casting Consortium at UIUC, including AK Steel, (Middletown, OH), Allegheny Ludlum, (Brackenridge, PA), Armco Inc. (Middletown, OH), BHP Co. Ltd. (Melbourne, Australia), Inland Steel Corp. (East Chicago, IN), LTV (Cleveland, OH), and Stollberg, Inc., (Niagara Falls, NY) for their continued support of our research and the National Center for Supercomputing Applications (NCSA) at the UIUC for computing time.

References

1. S.N. Singh and K.E. Blazek, J. Metals, 26 (1974), 17-27.
2. A. Grill, J. Brimacombe and F. Weinberg, Ironmaking Steelmaking, 3 (1) (1976), 38-47.
3. T. Saeki et. al., Tetsu to Hagane, 68 (13) (1982), 1773-1782.
4. H. Suzuki et. al., Trans. ISIJ, 24 (1984), 54-59.
5. C.H. Ye et. al., ISIJ Internat., 36 (1996), S159-S162.
6. H. Zhu, (PhD Thesis, University of Illinois, 1997).
7. A. Moitra, (Ph.D. Thesis, University of Illinois at Urbana-Champaign, 1993).
8. B. Ho, (Masters Thesis, University of Illinois at Urbana-Champaign, 1992).
9. H. Mizukami, K. Murakami and Y. Miyashita, Tetsu-to-Hagane, 63 (146) (1977), S 652.
10. A. Jablonka, K. Harste and K. Schwerdtfeger, Steel Research, 1 (1) (1991), 24-29.
11. I. Jimbo and A. Cramb, Metall. Trans. B, 24B (1993), 5-10.
12. P. Kozlowski et. al., Metall. Trans. A, 23A (March) (1992), 903-918.
13. P.J. Wray, Met. Trans., 13A (1) (1982), 125-134.
14. T. Suzuki et. al., Ironmaking Steelmaking, 15 (2) (1988), 90-100.
15. K. Nakai et. al., in Continuous Casting '85, (London, UK: Inst. Metals, 1985), paper 71.
16. M.M. Wolf, in PTD Proceedings, 13, (Warrendale, PA: Iron Steel Society, 1995), 99-117.
17. B.G. Thomas, J. Iron Steel Inst. Japan Internat., 35 (6) (1995), 737-743.
18. J.K. Brimacombe, F. Weinberg and E.B. Hawbolt, Metal. Trans. B, 10B (1979), 279-292.
19. A. Yamanaka et. al., Ironmaking Steelmaking, 22 (6) (1995), 508-512.